Cell Reports
Medicine

Article

GRP78-CAR T cell effector function against solid and brain tumors is controlled by GRP78 expression on T cells

Graphical abstract

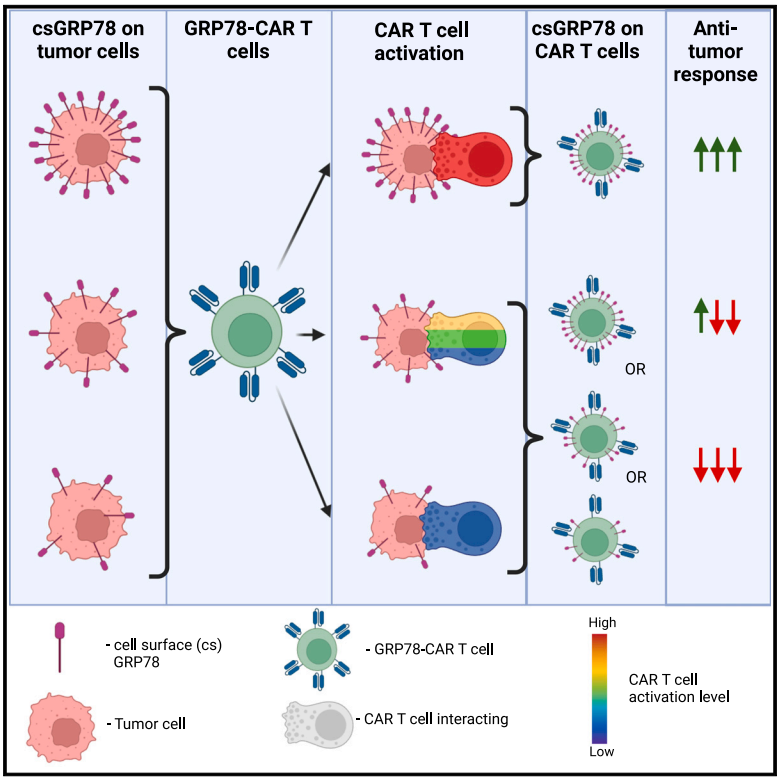

Highlights

- GRP78 is expressed among different pediatric solid and brain tumors
- GRP78-CAR T cells recognize and kill GRP78+ tumors
- Efficacy of GRP78-CAR T cells is mediated by GRP78 levels on tumor cells and T cells
- csGRP78 upregulation on CAR T cells is tumor-type dependent

Authors

Jorge Ibanez, Nikhil Hebbar, Unmesha Thanekar, ..., Jason Chiang, M. Paulina Velasquez, Giedre Krenciute

Correspondence

paulina.velasquez@stjude.org (M.P.V.), giedre.krenciute@stjude.org (G.K.)

In brief

Ibanez et al. describe that GRP78-CAR T cell therapy is a suitable option for pediatric solid and brain tumors with no toxicity in pre-clinical models. The anti-tumor activity of GRP78-CAR T cells is impacted by csGRP78 levels on tumors and by activation-induced csGRP78 on T cells.

Ibanez et al., 2023, Cell Reports Medicine *4*, 101297
November 21, 2023
https://doi.org/10.1016/j.xcrm.2023.101297

CellPress

Cell Reports Medicine

CellPress
OPEN ACCESS

Article

GRP78-CAR T cell effector function against solid and brain tumors is controlled by GRP78 expression on T cells

Jorge Ibanez,[1] Nikhil Hebbar,[1] Unmesha Thanekar,[1] Zhongzhen Yi,[1] Haley Houke,[1] Meghan Ward,[1] Chris Nevitt,[1] Liqing Tian,[1] Stephen C. Mack,[2] Heather Sheppard,[3] Jason Chiang,[3] M. Paulina Velasquez,[1,*] and Giedre Krenciute[1,4,*]

[1]Department of Bone Marrow Transplantation and Cellular Therapy, St. Jude Children's Research Hospital, 262 Danny Thomas Place, Memphis, TN 38105, USA

[2]Department of Developmental Neurobiology, St. Jude Children's Research Hospital, 262 Danny Thomas Place, Memphis, TN 38105, USA

[3]Department of Pathology, St. Jude Children's Research Hospital, 262 Danny Thomas Place, Memphis, TN 38105, USA

[4]Lead contact

*Correspondence: paulina.velasquez@stjude.org (M.P.V.), giedre.krenciute@stjude.org (G.K.)

https://doi.org/10.1016/j.xcrm.2023.101297

SUMMARY

Lack of targetable antigens is a key limitation for developing successful T cell-based immunotherapies. Members of the unfolded protein response (UPR) represent ideal immunotherapy targets because the UPR regulates the ability of cancer cells to resist cell death, sustain proliferation, and metastasize. Glucose-regulated protein 78 (GRP78) is a key UPR regulator that is overexpressed and translocated to the cell surface of a wide variety of cancers in response to elevated endoplasmic reticulum (ER) stress. We show that GRP78 is highly expressed on the cell surface of multiple solid and brain tumors, making cell surface GRP78 a promising chimeric antigen receptor (CAR) T cell target. We demonstrate that GRP78-CAR T cells can recognize and kill GRP78+ brain and solid tumors *in vitro* and *in vivo*. Additionally, our findings demonstrate that GRP78 is upregulated on CAR T cells upon T cell activation; however, this expression is tumor-cell-line specific and results in heterogeneous GRP78-CAR T cell therapeutic response.

INTRODUCTION

The anti-tumor activity of chimeric antigen receptor (CAR) T cells for solid and brain tumors is hampered by several factors including limited CAR T cell expansion and persistence, the immunosuppressive tumor microenvironment (TME), and heterogeneous expression of a limited array of targetable tumor antigens.[1,2] These factors have impacted the limited success of clinical trials for glioblastoma multiforme (GBM) and solid tumors.[3–7] Additionally, on-target/off-cancer toxicities have been observed in pre-clinical and clinical studies,[8,9] highlighting the need to identify tumor-specific antigens expressed on a broad range of tumors.

To achieve this, we set out to explore targeting cell surface glucose-regulated protein 78 (csGRP78) as a CAR T cell target for solid and brain tumors. GRP78 is a key unfolded protein response (UPR) regulator that normally resides in the endoplasmic reticulum (ER)[10] and is overexpressed and translocated to the cancer cell surface in several malignancies, including solid tumors, in response to elevated ER stress.[11,12] As a common essential gene (DepMap Portal, Broad Institute), GRP78 is less likely to be susceptible to antigen loss. In addition, the fact that the cell surface translocation of GRP78 in tumor cells is driven by multiple mechanisms[13–16] decreases the possibility of immune escape. All these features make GRP78 an extremely attractive target antigen for solid and brain tumors.

We have previously demonstrated that GRP78-CAR T cells have robust anti-tumor activity against acute myeloid leukemia (AML).[17] Here, we successfully target GRP78 on adult GBM (aGBM), diffuse intrinsic pontine glioma (DIPG), osteosarcoma (OS), triple-negative breast cancer (TNBC), and Ewing sarcoma (EWS). We show that the interaction of CAR T cells with different tumor cells results in varying degrees of T cell activation as determined by the calcium flux (Ca^{2+}) in GRP78-CAR T cells and interferon γ (IFN-γ) secretion. Interestingly, the level of T cell activation did not correlate with GRP78 expression level on tumor cells. Finally, we demonstrate that GRP78-CAR T cells exhibit different levels of anti-tumor activity across all tumors tested and that this activity might be dependent on csGRP78 expression on T cells.

RESULTS

GRP78 is expressed on the cell surface of solid and brain tumors

It has been previously shown that GRP78 is commonly expressed in many cancers.[18] Consistent with these data, our analysis of GRP78 (*HSPA5*) gene expression in The Cancer Genome Atlas (TCGA) database shows that the *HSPA5* gene is highly expressed in different cancers (Figure S1A). Expression in healthy tissues, on the other hand, is variable as judged by mRNA expression using the Genome Tissue Expression (GTEx) database (Figure S1B) and immunohistochemistry of healthy tissues

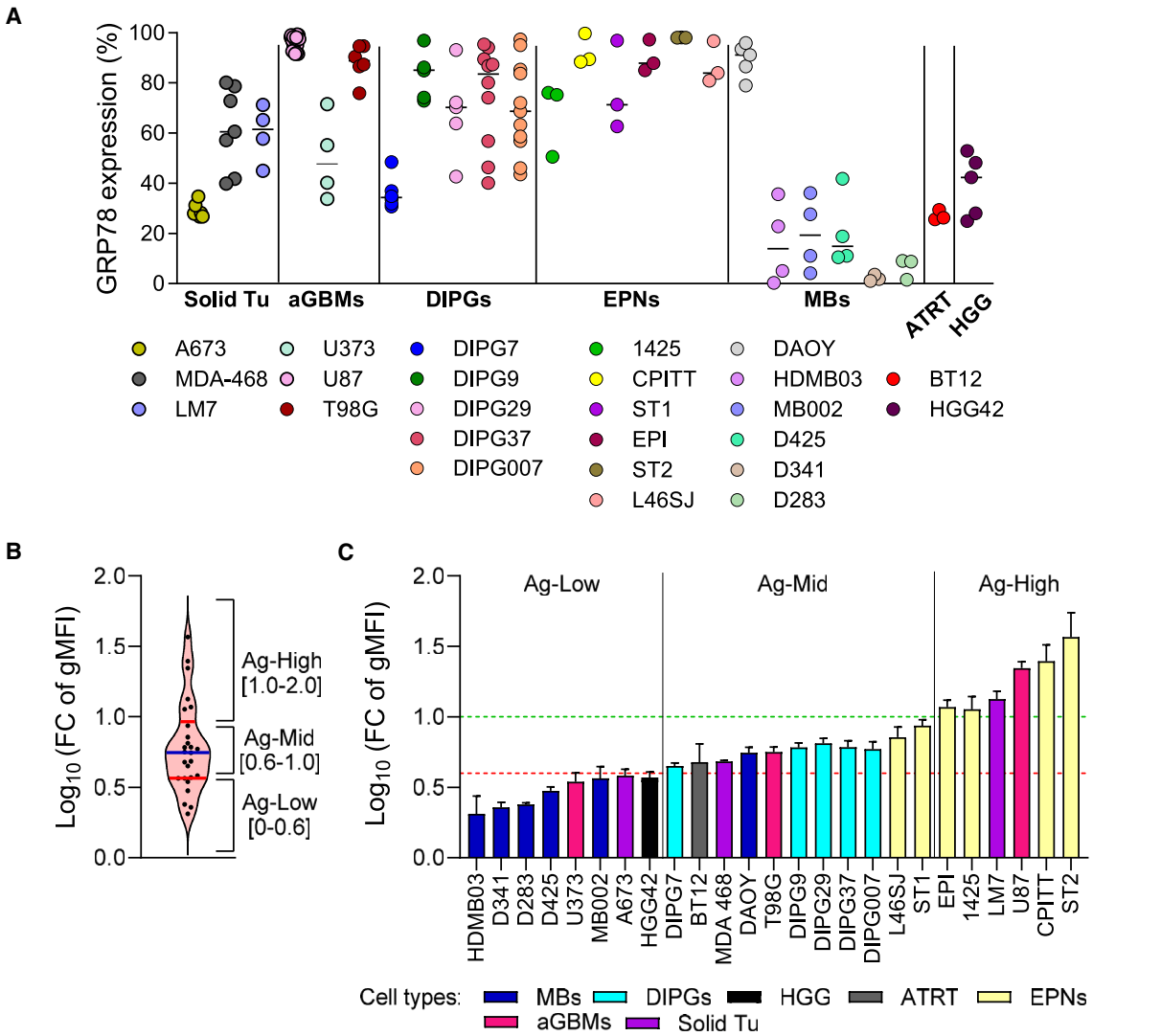

Figure 1. GRP78 is expressed on the cell surface of brain and solid tumors

(A) Cell surface GRP78 expression percentage in several pediatric (diffuse intrinsic pontine gliomas [DIPGs], ependymomas [EPNs], medulloblastomas [MBs], atypical teratoid rhabdoid tumor [ATRT], and high-grade glioma [HGG]) and adult brain tumors (adult glioblastoma multiforme [aGMBs]) and solid tumors (Solid Tus).

(B) Distribution of GRP78 expression levels among the samples tested in (A), presented as log10 transformed fold change of GRP78 geometric mean fluorescence intensity (gMFI) and their respective isotypes. Expression levels were defined by quartiles into low-GRP78-expressing cells (Ag-Low), middle-GRP78-expressing cells (Ag-Mid), and high-GRP78-expressing cells (Ag-Hi).

(C) Distribution of the cell lines tested in (A) regarding their relative GRP78 expression levels defined in (B). Red and green lines define cutoffs at 0.6 and 1, respectively. n = 3–21. Mean and SEM are shown.

(Figure S2). However, these analyses do not provide information about the localization of GRP78, which needs to be expressed on the cell surface for effective CAR T cell therapy. To evaluate GRP78 suitability as a CAR T cell target for solid and brain tumors, we first validated its surface expression on a panel of solid tumors (A673, LM7, MDA-MB-468 [MDA-468 hereafter]), adult brain tumors (U87, U373, T98G), and pediatric patient-derived brain tumor cell lines (DIPGs [DIPG7, DIPG9, DIPG29, DIPG37, DIPG007]; ependymomas [1425, CPITT, ST1, ST2, EPI, L46SJ]; medulloblastoma [DAOY, HDMBO3, MB002, D425, D341, D283]; high-grade glioma [HGG42]; and atypical teratoid rhabdoid tumor [ATRT (BT12)]) using flow cytometry (Figures 1A and S3A). GRP78 cell surface expression was differentially elevated in all cell lines tested, with the highest expression on U87 and ependymomas and the lowest on A673 and medulloblastoma cells, except DAOY (Figures 1A and 1C). These findings correlated with GRP78 gene expression in the St. Jude Cloud[19] and TARGET Childhood Cancer Program (available at the Genomic Data Commons [https://portal.gdc.cancer.gov]) databases (Figure S3B), bulk RNA sequencing (RNA-seq) data of the cell lines used in the study (Figure S3C), and immunohistochemistry of selected pediatric brain tumors

(Figure S4). Based on csGRP78 expression data, we next established a hierarchy of csGRP78 expression in different tumor cells used in the study: high-csGRP78-expressing cells (ST2, CPITT, U87, LM7, EPI, 1425), middle-expressing cells (ST1, L46SJ, DIPG7, DIPG29, DIPG37, DIPG9, DIPG007, T98G, DAOY, MDA468), and low-expressing cells (BT12, MB002, A673, HGG42, BT16, U373, D425, HDMBO3, D283, and D341) (Figures 1B and 1C).

GRP78-CAR T cells target GRP78+ brain and solid tumor cells and secrete cytokines *in vitro*

To evaluate GRP78 antigen specificity, we transduced activated T cells either with a second-generation GRP78-specific CAR (GRP78)[17] or a non-signaling control CAR (Ctrl) lacking the costimulatory and intracellular signaling domains (Figure S5A). CAR expression was confirmed using flow cytometry, and both CAR constructs were efficiently expressed on the T cell surface (range: 70.1–95.3) (Figure S5B). There was no difference in the proportion of CD4/CD8 or the memory phenotype of GRP78-CAR T cells when compared with Ctrl-CAR or non-transduced (NT) cells (Figure S5C).

We then evaluated the function of the CAR T cells against GRP78-expressing tumor lines by assessing (1) cytolytic potential, (2) proliferative capacity, and (3) cytokine secretion. To evaluate the cytolytic potential of GRP78-CAR T cells, we performed a 24-h MTS-based cytotoxicity assay against U87, U373, T98G, MDA-468, DIPG7, DIPG9, DIPG29, DIPG37, and DIPG007. U87 and MDA-468 cells were effectively killed at the lowest effector-to-target (E:T) ratio of 0.5:1, whereas A673 cells only exhibited a partial response (Figure 2A), consistent with their high and low relative levels of GRP78 surface expression (Figure 1C). DIPG cell killing by GRP78-CAR T cells was much more variable. GRP78-CAR T cells failed to kill DIPG7, despite having GRP78 expression in the middle range (40%–50%) (Figure S6A). Next, to demonstrate the proliferative capacity of GRP78-CAR T cells in response to chronic antigen exposure, we performed a repeat stimulation assay.[20] GRP78-CAR T cells killed tumor cells and expanded for up to 4 successive stimulations in the presence of U87 cells (Figure 2B), while A673, MDA-468 (Figure 2B), and DIPGs (Figure S6B) failed to expand post-first or -second stimulations. We also observed significant CAR T cell expansion and sequential killing for up to 5 stimulations upon exposure to other brain tumor cell lines, U373 and T98G (Figures S6A and S6B).

Upon chronic antigen exposure to U87 cells, CAR T cells enriched for CD8 and effector memory phenotypes (CCR7−, CD45RA−), with high levels of PD-1, LAG-3, and TIM-3 (Figures S7A–S7D), suggesting that U87 cells highly activate CAR T cells. In the presence of DIPGs, PD-1, LAG-3, and TIM-3 were not upregulated after the first stimulation (Figures S7E and S7F), which correlated with their impairment to proliferate when compared with U87 cells (Figures S7G and S7H).

To further evaluate effector function of GRP78-CAR T cells, we measured cytokine secretion upon antigen stimulation. We collected supernatants 24-h post-first CAR T cell and tumor cell (U87, MDA-468, A673, DIPG7, DIPG29, DIPG37, and DIP007) co-cultures and examined the levels of Th1/Tc1 (IFN-γ, tumor necrosis factor α [TNF-α], granulocyte macrophage colony-stimulating factor [GM-CSF], interleukin-2 [IL-2]), Th2/Tc2 (IL-4, IL-5, IL-6, IL-10, IL-13), and other cytokines (RANTES, IP-10) using multiplex cytokine array. GRP78-CAR T cells produced high levels of Th1/Tc1 cytokines, with U87 cells eliciting the most robust response, followed by MDA-468 cells (Figures 2D, 2E, and S8). In comparison, IFN-γ, GM-CSF, and IL-2 levels were significantly lower in response to DIPGs and A673 cells (Figures 2E and S8). A673 and DIPGs co-cultures resulted in high levels of the pro-inflammatory cytokine IP-10, which was not seen in response to U87 or MDA-468 cells (Figures 2E and S8).

GRP78-CAR T cells show potent anti-tumor activity in multiple *in vivo* models

To interrogate the *in vivo* safety and potency of GRP78-CAR T cells, we tested GRP78-CAR T cells in non-tumor-bearing mice and against several xenograft models, respectively. We first evaluated the safety of GRP78-CAR T cells. We show that our human GRP78-CAR T cells can recognize murine GRP78 (Figure S9; Hebbar et al.[17]), providing the rationale to test safety in non-tumor-bearing NSG animals. We injected 10^7 GRP78-CAR T cells co-transduced with GFP.ffluc intravenously (i.v.) into non-tumor-bearing NSG mice, and we tracked their expansion by bioluminescence for 1 week (Figure S10A). Our results show a transient increase of Ctrl- and GRP78-CAR T cells on day 1 with no statistically significant difference between the groups (Figures S10B–S10D), demonstrating successful T cell injection. CAR T cells started contracting on day 2 and were undetectable by day 6–8. There were no changes in animal weight, and pathology analysis of vital organs did not find any damage post-CAR T cell treatment (Figures S10C–S10E), suggesting that GRP78-CAR T cells are safe.

We next evaluated the therapeutic benefit of GRP78-CAR T cells in different tumor models that express high, middle, and low levels of csGRP78. First, we evaluated the *in vivo* anti-tumor response against an orthotopic GBM model (U87, high csGRP78 expression). On day 0, U87.GFP.ffluc cells (3×10^4) were implanted intracranially (i.c.) in the brain cortex, followed by a single i.c. dose of 2×10^6 GRP78- or Ctrl-CAR T cells 7 days later (Figure 3A). GRP78-CAR treatment resulted in sustained disease control in all animals in the treatment group (Figures 3B, 3C, and S11A).

Next, we tested the *in vivo* efficacy against an OS (LM7, high csGRP78 expression) model. 1×10^6 LM7.GFP.ffluc was injected intraperitoneally (i.p.), and 7 days later, mice received a single i.p. dose of 5×10^5 GRP78- or Ctrl-CAR T cells (Figure 3D). 4 out of 5 mice treated with GRP78 reached complete remission within the first 3 weeks of treatment (Figures 3E, 3F, and S11B), and 2 out of 5 mice demonstrated long-term (>100 days) complete response resulting in a significant overall survival.

Then, we tested the *in vivo* efficacy against the orthotopic TNBC model (MDA-468, middle csGRP78 expression). MDA-468.GFP.ffluc cells (5×10^5) were injected into the mammary fat pad of NSG mice, and on day 7, mice received a single i.v. dose of 3×10^6 GRP78- or Ctrl-CAR T cells (Figure 3G). GRP78-CAR T cell-treated mice achieved complete remission

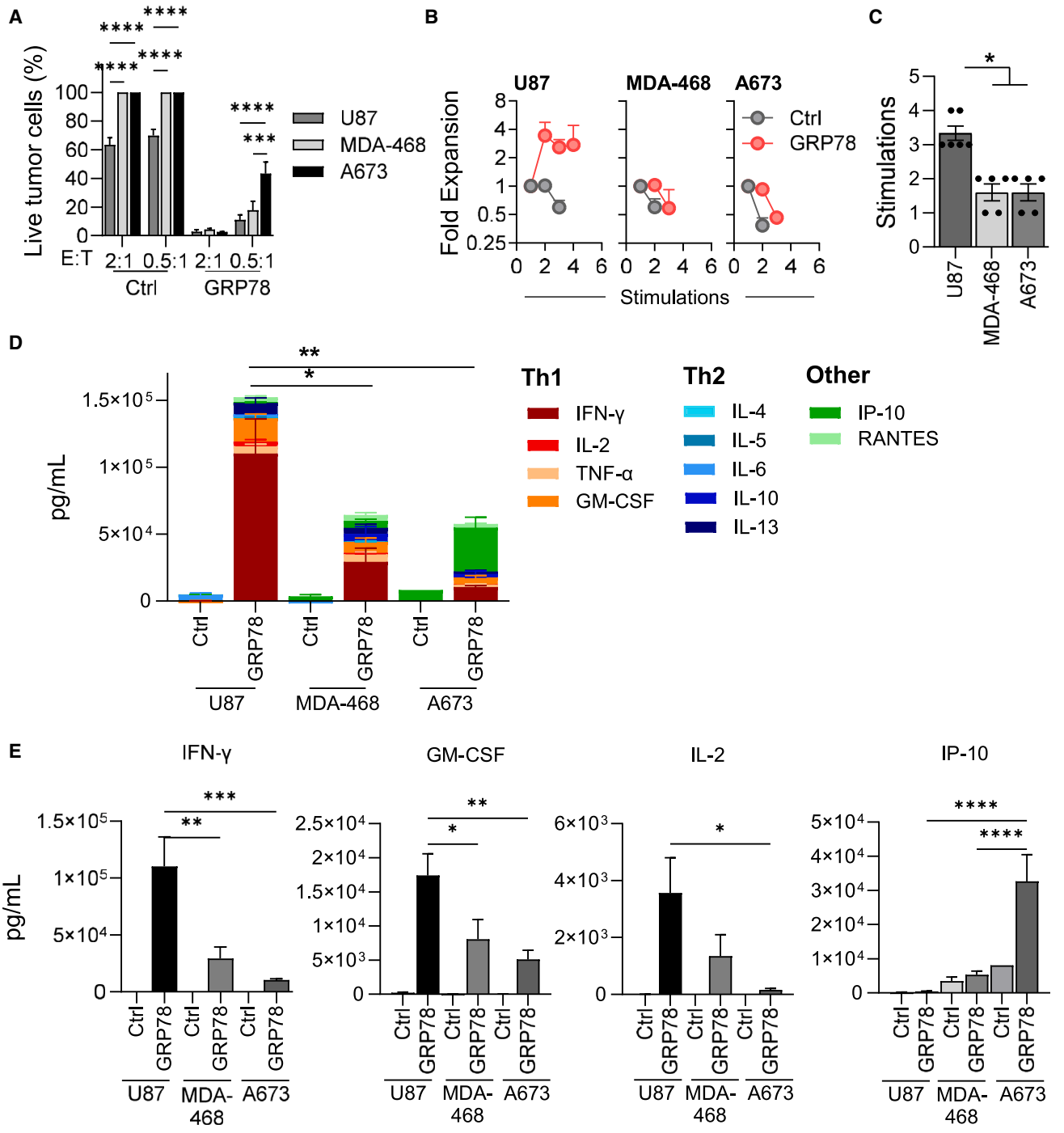

Figure 2. GRP78-CAR T cells recognize GRP78+ glioblastoma multiforme and solid tumor cells *in vitro*

(A) MTS-based cytotoxicity assay of GRP78-CAR T cells or Ctrl-CAR T cells against U87, MDA-468, and A673 cells at two different E:T ratios (n = 3, two-way ANOVA, Tukey's test, ***p = 0.0002 and ****p < 0.0001).

(B) Serial stimulation assay using effector T cells (GRP78-CAR or Ctrl-CAR T cells) against U87 (n = 6), MDA-468 (n = 5), and A673 (n = 5) target cells at 2:1 E:T ratio. Fresh target cells were added every 72–96 h.

(C) Representation of maximal number of stimulations at which CAR T cells were able to expand and kill fresh GRP78+ tumor cells in (B).

(D) Summary plots of cytokine production by GRP78-CAR T cells or Ctrl-CAR T cells in the supernatant when cultured with U87, MDA-468, and A673 cells at 2:1 E:T ratio after 24-h stimulation. Cytokines were measured by using MILLIPLEX cytokine assay (n = 3–5, one-way ANOVA, Sidak multiple comparison test, *p < 0.05 and **p < 0.005).

(E) Representation of values for selected cytokines (IFN-γ, GM-CSF, IL-2, IP-10) from (D) (n = 3–5, one-way ANOVA, Sidak multiple comparison test, *p < 0.05, **p < 0.005, ***p < 0.001, and ****p < 0.0001). Mean and SEM are shown.

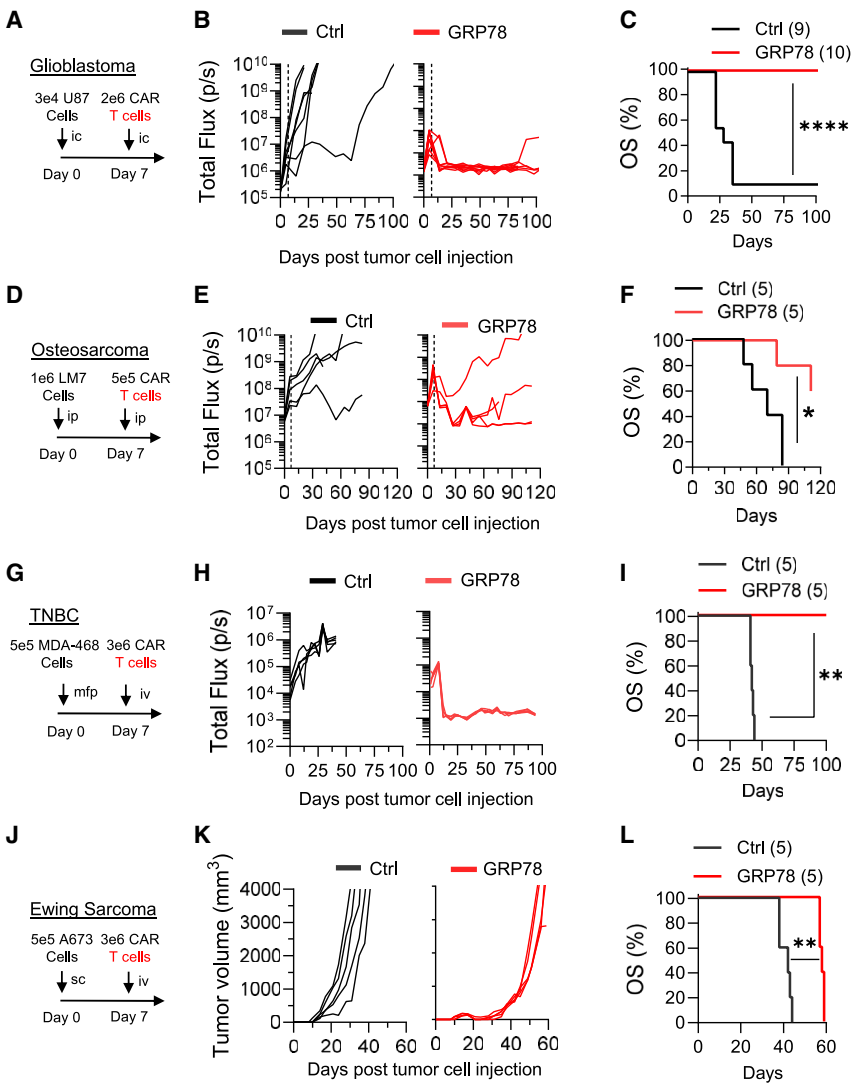

Figure 3. GRP78-CAR T cells show potent anti-tumor activity against solid and brain tumor xenograft models

(A) Schematic of the *in vivo* experimental design for GBM intracranial implant model. U87 cells (3×10^4) were implanted intracranially (i.c.) into in the brain cortex, followed by a single i.c. dose of 2×10^6 GRP78- or Ctrl-CAR T cells 7 days post-tumor injection.

(B) Total flux from tumor cells in all mice treated with CAR T cells. The tumors were measured weekly using bioluminescence imaging.

(C) Kaplan-Meier survival analysis of mice treated with CAR T cells (log-rank [Mantel-Cox] test, n = 9–10, ****$p < 0.0001$).

(D) Schematic of the *in vivo* experimental design for osteosarcoma intraperitoneal (i.p.) model. LM7 cells (1×10^6) were implanted i.p. followed by a single i.p. dose of 5×10^5 GRP78- or Ctrl-CAR T cells 7 days post-tumor injection.

(E) The tumors were measured weekly using bioluminescence imaging.

(F) Kaplan-Meier survival analysis of mice treated with CAR T cells (log-rank [Mantel-Cox] test, n = 5, *$p = 0.016$).

(G) Schematic of the *in vivo* experimental design for TNBC orthotopic xenograft model. MDA-468 cells (0.5×10^6) were injected orthotopically into the mammary fat pads of NSG mice. 3×10^6 T cells were given intravenously (i.v.) on day 7 after tumor injection.

(H) Total flux from tumor cells in all mice treated with CAR T cells. The tumors were measured twice weekly using bioluminescence imaging.

(I) Kaplan-Meier survival analysis (log-rank [Mantel-Cox] test, n = 5, **$p = 0.0017$).

(J) Schematic of the *in vivo* experimental design for EWS xenograft model. 5×10^5 A673 (EWS) cells were injected subcutaneously (s.c.) into the flanks of NSG mice. The tumors were measured twice weekly using caliper measurements. 3×10^6 T cells were given i.v. on day 7 after tumor injection.

(K) Tumor volume (mm^3) as determined by caliper measurements (n = 5, $p < 0.05$).

(L) Kaplan-Meier survival analysis (log rank [Mantel-Cox] test, n = 5, **$p = 0.0012$).

within 2 weeks of T cell injection and remained tumor free for ~3 months until the end of the experiment. Mice treated with Ctrl-CAR T cells had disease progression (Figures 3H, 3I, and S11C). We then tested a second mid-csGRP78-expressing model, DIPG007. DIPG007.YFP.ffluc cells (1×10^6) were implanted i.c. in the brain cortex, followed by a single i.c. dose of 2×10^6 GRP78- or Ctrl-CAR T cells 7 days later (Figure S12A). In this model, the anti-tumor response was transient with no difference in the overall survival when compared with control (Figures S12B–S12D).

Lastly, we tested the *in vivo* efficacy of GRP78-CAR T cells against low-csGRP78-expressing tumor cells A673 (EWS). In the subcutaneous (s.c.) EWS xenograft model, mice were injected with 5×10^5 A673 cells s.c. on day 0 and received one single i.v. dose of 3×10^6 GRP78-CAR T cells on day 7 (Figure 3J). Mice treated with GRP78-CAR T cells had reduced tumor volumes compared with treatment groups and resulted in delayed tumor growth (Figures 3K and 3L). However, none of the animals treated achieved complete remission.

Intracellular Ca^{2+} signaling does not correlate with GRP78-CAR T cell response

Although csGRP78 is expressed in all of the cell lines tested in this study, there were significant differences in the CAR T cell efficacy against each tumor cell line in terms of expansion, cytokine secretion, and tumor killing *in vitro* and *in vivo*. We posited that varied antigen densities on different tumors elicited changes in the activation potential of GRP78-CAR T cells. To demonstrate these changes, we used live-cell imaging to measure intracellular Ca^{2+} flux as an indicator of CAR T cell activation. Ctrl-CAR and GRP78-CAR T cells were labeled with Cal-520AM, a fluorescent calcium-sensitive dye. During the interaction with antigen-presenting tumor cells, CAR T cells undergo change of green fluorescence intensity, which indicates the levels of

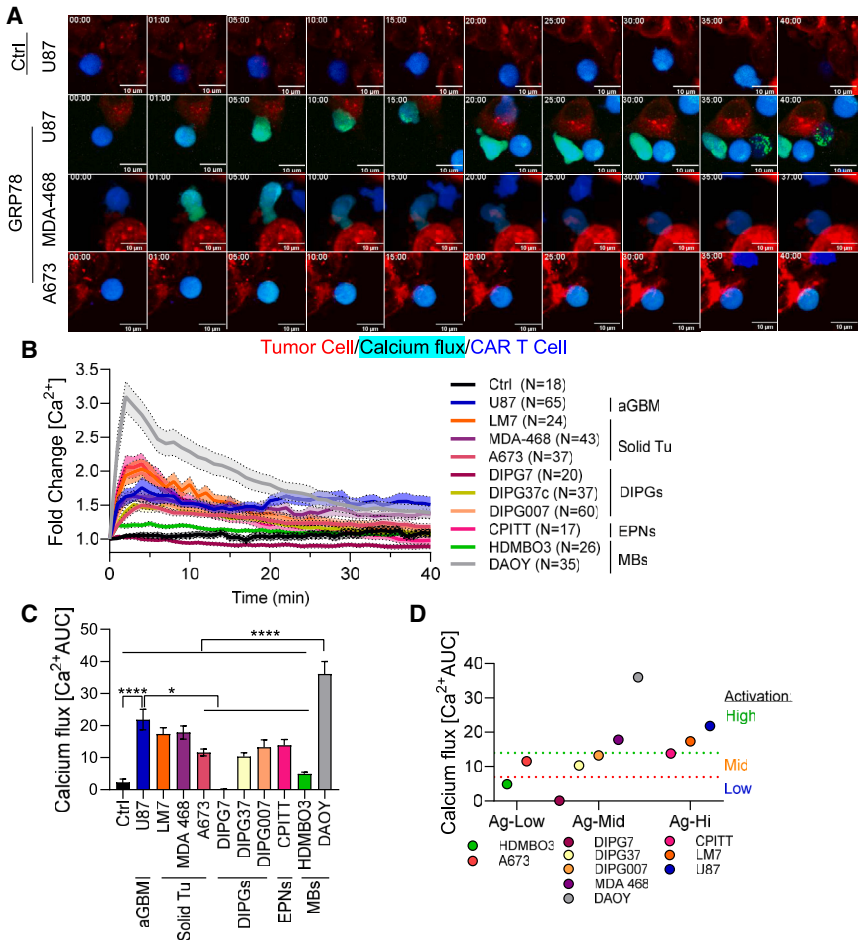

Figure 4. Activation potential of GRP78-CAR T cells is cell-line dependent

(A) Representative time lapse images of GRP78- or Ctrl-CAR T cells interacting with U87, MDA-468, or A673 tumor cells acquired by spinning disc confocal live-cell imaging. CAR T cells were labeled with CellTrace violet (blue) and CAL520 (green), and tumor cells were labeled with CellTracker Red-CMTPX (red). Scale bar: 10 μm.

(B) Quantification of calcium flux in CAR T cells upon tumor cell interaction shown in (A).

(C) Quantification of total calcium flux as area under the curve (AUC) (n = 2–3, cells = 17–65; one-way ANOVA, Tukey's test, ****$p < 0.0001$ and *$p < 0.05$). Mean and SEM are shown.

(D) Stratification of calcium flux response (Ca^{2+}AUC) by the relative expression of GRP78 on the cell surface of tumor cells.

intracellular Ca^{2+} mobilization. As expected, only the functional GRP78-CAR T cells were able to trigger Ca^{2+} flux (Figure 4A). GRP78-CAR T cells interacting with high-GRP78-expressing cell lines (U87, CPITT, LM7) were able to sustain the Ca^{2+} flux for longer time periods (<40 min), whereas CAR T cells interacting with middle-csGRP78-expressing cells (DIPG37, DIPG007, DIPG7, MDA-468) failed to maintain calcium influx for an equivalent amount of time (>20 min). Low cell surface csGRP78-expressing tumor cells, such as A673 and HDMB03, failed to activate GRP78-CAR T cells (Figures 4A, 4B, and S13). An area under the curve (AUC) analysis revealed that GRP78-CAR T cells interacting with DAOY or U87 resulted in the most sustained intracellular Ca^{2+} mobilization, followed by ependymoma (CPITT), LM7, and 468 (Figures 4C and S13). Plotting Ca^{2+} flux vs. low, middle, and high csGRP78 expression shows no correlation between the antigen level and the calcium response (Figures 4D and S14A). We also measured the IFN-γ secretion after 24-h co-culture against the same tumor cell lines we used for imaging studies. Consistent with our imaging findings, our results show that IFN-γ secretion follows the same pattern as the Ca^{2+} flux (Figure S14B) and that there is no correlation between IFN-γ secretion and csGRP78 expression levels on tumor cells (Figure S14C).

Tumor cells control GRP78 expression on CAR T cells

We previously showed that csGRP78 is expressed on activated T cells (Hebbar et al.[17]; Figures S15A and S15B); however, this was tested with plate-bound anti-CD3/CD28 activation and not with tumor-bound antigen. Thus, we next decided to evaluate whether GRP78 is expressed on T cells in a tumor-dependent manner, which might be contributing to the variation in CAR T cell activity. We tested here the level of csGRP78 expression on T cells post-co-culture with different csGRP78-expressing tumor cells. 24 hours after co-culture setup, we collected CAR T cells and determined csGRP78 expression via flow cytometry. Interestingly, co-cultures with non-functional Ctrl-CAR T cells and tumor cells already show some csGRP78 expression on T cells, and the level of csGRP78 was tumor-cell-line specific (Figures 5A and 5B). Co-culture with GRP78-CAR T cells and tumor cells showed even higher csGRP78 expression on T cells (Figures 5A and 5B); however, there was no correlation between csGRP78 expression on tumor cells and on T cells (Figure 5C). These findings suggest that csGRP78 expression on T cells is controlled by both T cell activation and tumor-cell-specific factor(s).

Given the fact that GRP78 is expressed on activated T cells, this can lead to GRP78-CAR T cell fratricide, or self-killing. To test this, we activated NT T cells *in vitro* to induce the expression of csGRP78 at the T cell surface and then co-cultured them with either Ctrl- or GRP78-CAR T cells. We then evaluated the ability of the GRP78-CAR T cells to kill the activated NT T cells. Our results show that activated T cells can be recognized and killed by GRP78-CAR T cells but not by Ctrl-CAR T cells (Figures S15C and S15D). Together, these findings suggest that GRP78-CAR T cell interaction with tumor cells leads to upregulation of csGRP78 on CAR T cells, giving rise to fratricidal CAR T activity, and that this might be the reason that these CAR T cells have

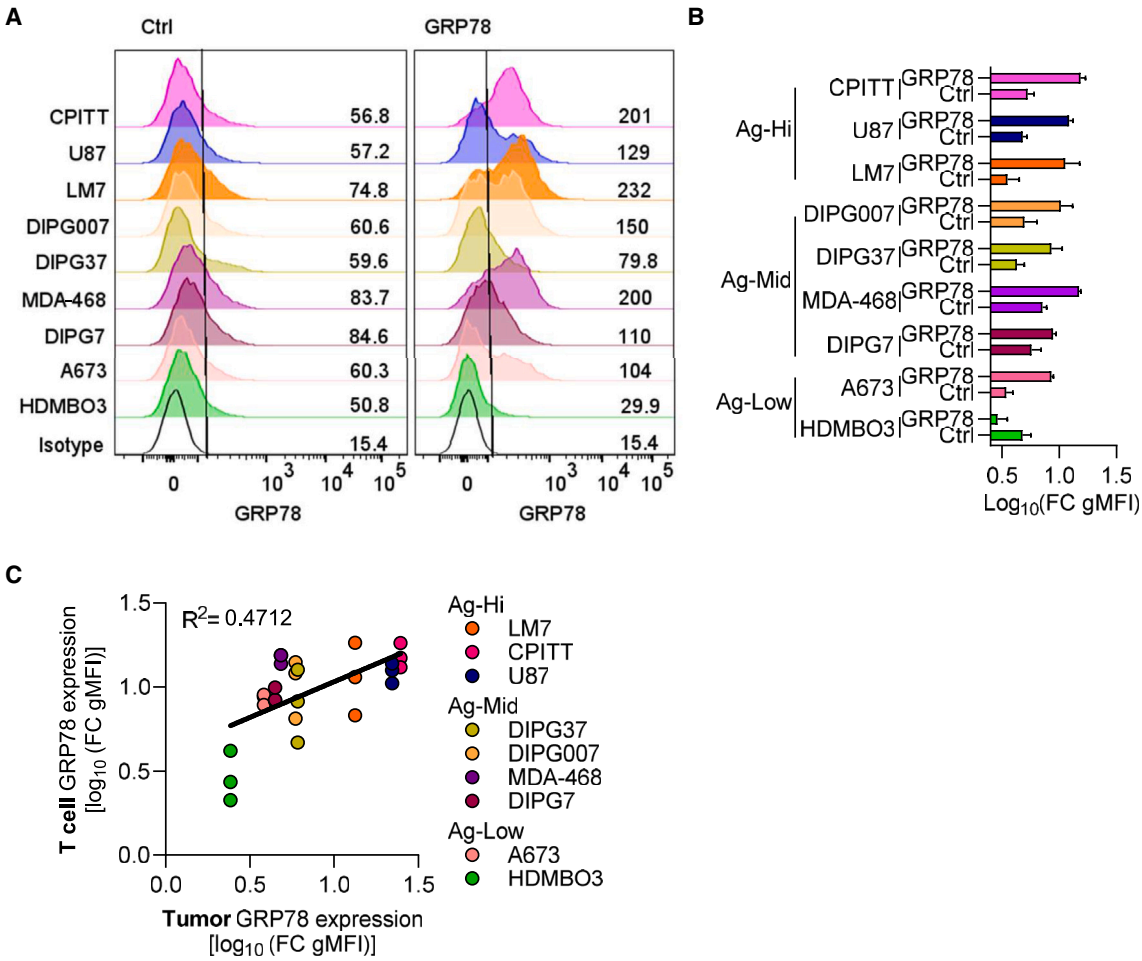

Figure 5. Tumor cells control GRP78 expression on CAR T cells

(A) Representative histogram plots of GRP78 expression on T cells after co-culture with tumor cells for 24 h, evaluated by flow cytometry. Lines define isotype control, and gMFIs are listed for each sample.

(B) Quantification of normalized GRP78 expression levels on T cells in (A) (n = 3). Mean and SEM are shown.

(C) Linear correlation of GRP78 expression on T cells (after co-culture with tumor cells) vs. GRP78 expression on tumor cells.

limited anti-tumor response *in vivo* in tumors expressing low to middle levels of GRP78, such as DIPGs and EWS.

Overcoming limited GRP78-CAR T cell response

To overcome the limited *in vivo* anti-tumor response of GRP78-CAR T cells against DIPGs (Figure S12), we first decided to increase the T cell dose (Figure S16A). The higher T cell dose improved the tumor control and overall survival, but all tumors relapsed 2 weeks after the treatment (Figures S16B and S16D), suggesting that further optimizations are needed. We next tested the knockout (KO) of RAS P21 protein activator 2 (RASA2) in GRP78-CAR T cells. We have previously shown that KO of RASA2 can improve CAR T cell response in instances where target antigen is expressed at low levels.[21] We generated RASA2 KO GRP78-CAR T cells and tested their activity *in vivo*-against DIPG (Figure S16E). We found that RASA2 KO GRP78-CAR T cells were highly effective in controlling tumor burden when compared with Ctrl KO GRP78-CAR T cells (Figures S16F–S16H). These results suggest that KO of RASA2 improved GRP78-CAR T cell activity when targeting tumors with low GRP78 expression.

It is important to note that generating RASA2 KO GRP78-CAR T cells via electroporation (regardless of guide RNAs [AAVS1 or RASA2] used) highly affected GRP78-CAR T cell viability. This was most likely due to the increased GRP78 expression on T cells owing to electroporation-induced stress,[22] which most likely led to an increase of GRP78-CAR T cell fratricidal activity. To overcome this, we used 50 nM dasatinib[23] after 3 days of transduction to transiently inhibit CAR T cell activation and preserve CAR T cell viability and expansion. The implication of this observation is addressed in the discussion.

DISCUSSION

Here, we demonstrate that csGRP78 is expressed in solid and brain tumors, making GRP78 an attractive target for T cell

therapies. We show that GRP78-CAR T cells have potent anti-tumor activity against solid and brain tumor cells *in vitro* and *in vivo*. We also demonstrate that GRP78 is expressed on activated T cells and that its expression is not dependent on antigen density but is rather tumor-cell-type dependent.

Previously, our group designed a second-generation GRP78-CAR endowed with a peptide-based antigen recognition domain and successfully targeted GRP78 on the surface of AML.[17] Additionally, a recent report showed that GRP78-CAR T cells are effective against adult GBM *in vitro* and *in vivo*.[24] Building on these findings, we have identified GRP78 as a target antigen that is selectively overexpressed on the surface of many solid and brain tumors. Here, we determined surface GRP78 expression using flow cytometry in a panel of diverse tumor types including GBM, DIPGs, ependymomas (EPNs), medulloblastomas (MBs), OS, HGG, ATRT, TNBC, and EWS. We show that GRP78-CAR T cells specifically recognize and kill tumor cells *in vitro* when csGRP78 is expressed at mid to high levels. *In vivo*, we found that only high-level-GRP78-expressing cells consistently responded to CAR T cell treatment. Low- and mid-level-GRP78-expressing cell lines had mixed response to GRP78-CAR T cell treatment. Interestingly, we found that GRP78 is expressed on CAR T cells not only after T cell activation but also upon interaction with tumor cells. Tumor cells that induced the highest GRP78 expression on CAR T cells showed minimal response to GRP78-CAR T cell treatment, such as DIPG. These new findings align with prior literature indicating GRP78's biological role in T cell signaling and effector function.[24]

Our data show that CAR T cells express higher levels of csGRP78 after exposure to DIPG cells compared with other cell types. Given that DIPGs are known to be highly immunosuppressive,[25] we hypothesize that the interaction between GRP78-CAR T and DIPG cells leads to ER stress in T cells, potentially through tumor-derived extracellular vesicles (TEVs), reactive oxygen species (ROS), or lactic acid, as has been shown for solid tumors.[26–31] This leads to upregulation of GRP78 in CAR T cells and concomitant translocation of GRP78 to the cell surface, ultimately leading to GRP78-CAR T cell fratricide and dampened T cell effector function against DIPGs. However, additional studies are needed to validate this hypothesis and will be the focus of follow-up publications. We also observed increased csGRP78 expression upon electroporation of T cells. ER stress has been previously observed from electroporation procedures,[22] which explains the upregulation of csGRP78 in electroporated T cells. Following transduction with the GRP78-CAR, this leads to low T cell viability and highly reduced expansion of gene-edited/electroporated GRP78-CAR T cells. Taken together, our and published data suggest that an ER-stress-induced increase in GRP78 surface translocation is a major inhibitor of T cell effector function. More in-depth mechanistic studies are warranted to better understand the extent of the impact and how it can be overcome for GRP78-CAR T cells.

While we show that GRP78-CAR T cells have potent anti-tumor activity against multiple solid and brain tumors, GRP78 expression on healthy tissues and activated T cells pose on-target/off-tumor toxicity concerns that could potentially limit GRP78-CAR utility. However, given recent advances in the production of next-generation CAR T cells, there are alternative options where targeting GRP78 can be beneficial for CAR T cells. For example, GRP78 could be targeted as part of a dual-targeting approach where the second antigen is used to enhance CAR T cell activation rather than cytolytic effect. More specifically, GRP78 could be considered a target for the CAR.BiTE[32] or switch receptor approaches.[33] For the latter, the extracellular portion of a receptor recognizes widely expressed molecules or surface proteins, but the intracellular region is engineered to provide a co-stimulatory signal to improve T cell activation. For example, the extracellular anti-GRP78 peptide and the transmembrane domain of the GRP78-CAR could be fused with only the intracellular 4-1BB signaling domain. When co-transduced with a different cytolytic signaling CAR, this strategy would induce better T cell activation in instances where the cytolytic CAR target is expressed at low levels, GRP78 is expressed at middle to high levels, and T cell anti-tumor response is incomplete with just the cytolytic CAR alone. Thus, while using GRP78 as a direct CAR T cell target might not be ideal for all solid and brain tumors, it is an ideal target for engineering next-generation, improved CAR T cells.

In conclusion, GRP78-CAR T cells have potent anti-tumor activity in both brain and solid tumors. GRP78 is a unique target that provides a feasible option for single, combinatorial, or other alternative approaches to CAR T cell therapy. We further conclude that GRP78 expression on T cells may play a crucial role in T cell biology and anti-tumor function, and investigating this further will be the focus of future work.

Limitations of the study

Our study findings underline the importance of gaining a more in-depth understanding of the effect of csGRP78 upregulation on T cell biology and CAR T cell effector function. In addition, the mechanism by which GRP78 is translocated to T cell surface is still not clear. While we speculate, based on our findings and published data, that ER stress plays a role in GRP78 cell surface translocation, further mechanistic studies are needed. We have also not yet determined the csGRP78 expression threshold on T cells at which GRP78-CAR will recognize a target. This information will be useful in optimizing GRP78-CAR T cell function and in developing mechanisms by which T cell fratricide can be circumvented. Finally, the current study is only focused on testing a second-generation GRP78-CAR with CD28.ζ signaling. Therefore, the role of other co-stimulatory domains, such as 41BBL or OX40, in csGRP78 expression on T cells and the anti-tumor efficacy of GRP78-CAR T cells remain unanswered. While we recognize that our current work does not address these issues, they will be incorporated into future efforts.

STAR★METHODS

Detailed methods are provided in the online version of this paper and include the following:

- KEY RESOURCES TABLE
- RESOURCE AVAILABILITY
  - Lead contact
  - Materials availability
  - Data and code availability

SUPPLEMENTAL INFORMATION

Supplemental information can be found online at https://doi.org/10.1016/j.xcrm.2023.101297.

ACKNOWLEDGMENTS

Surgeries and pre-clinical imaging were performed by the Center for In Vivo Imaging and Therapeutics, which is supported in part by National Institutes of Health (NIH) grants P01CA096832 and R50CA211481. Sequencing was performed by the Hartwell Center, which is supported in part by the National Cancer Institute (NCI)/NIH grant P30CA021765. Flow analysis was in part conducted by the Flow Cytometry and Cell Sorting Shared Resource. This work was supported by the Assisi Foundation of Memphis, the American Lebanese Syrian Associated Charities (ALSAC), a ChadTough Defeat DIPG Foundation grant to G.K., R01NS122859 to G.K., and the American Brain Tumor Association (ABTA) Basic Research Fellowship (supported by Humor to Fight the Tumor) to J.I.

AUTHOR CONTRIBUTIONS

Conceptualization, J.I., N.H., M.P.V., and G.K.; data analysis, J.I., N.H., Z.Y., H.H., U.T., M.W., C.N., L.T., H.S., J.C., M.P.V., and G.K.; investigation, J.I., N.H., Z.Y., H.H., U.T., and C.N.; resources, S.C.M., M.P.V., and G.K.; formal analysis, J.I., N.H., Z.Y., H.H., U.T., M.P.V., and G.K.; writing – original draft, J.I., N.H., M.P.V., and G.K.; writing – review & editing, J.I., M.W., M.P.V., and G.K.; funding acquisition, M.P.V., G.K., and J.I.; supervision, M.P.V. and G.K.

DECLARATION OF INTERESTS

N.H. and M.P.V. are named inventors on a patent application related to GRP78-CAR. N.H., G.K., and M.P.V. have other patent applications in the field of immunotherapy unrelated to this work.

INCLUSION AND DIVERSITY

We support inclusive, diverse, and equitable conduct of research.

Received: August 25, 2022
Revised: August 25, 2023
Accepted: October 26, 2023
Published: November 21, 2023

REFERENCES

1. Martinez, M., and Moon, E.K. (2019). CAR T Cells for Solid Tumors: New Strategies for Finding, Infiltrating, and Surviving in the Tumor Microenvironment. Front. Immunol. *10*, 128.
2. Rafiq, S., Hackett, C.S., and Brentjens, R.J. (2020). Engineering strategies to overcome the current roadblocks in CAR T cell therapy. Nat. Rev. Clin. Oncol. *17*, 147–167.
3. Ahmed, N., Brawley, V., Hegde, M., Bielamowicz, K., Kalra, M., Landi, D., Robertson, C., Gray, T.L., Diouf, O., Wakefield, A., et al. (2017). HER2-Specific Chimeric Antigen Receptor-Modified Virus-Specific T Cells for Progressive Glioblastoma: A Phase 1 Dose-Escalation Trial. JAMA Oncol. *3*, 1094–1101.
4. Brown, C.E., Alizadeh, D., Starr, R., Weng, L., Wagner, J.R., Naranjo, A., Ostberg, J.R., Blanchard, M.S., Kilpatrick, J., Simpson, J., et al. (2016). Regression of Glioblastoma after Chimeric Antigen Receptor T-Cell Therapy. N. Engl. J. Med. *375*, 2561–2569.
5. O'Rourke, D.M., Nasrallah, M.P., Desai, A., Melenhorst, J.J., Mansfield, K., Morrissette, J.J.D., Martinez-Lage, M., Brem, S., Maloney, E., Shen, A., et al. (2017). A single dose of peripherally infused EGFRvIII-directed CAR T cells mediates antigen loss and induces adaptive resistance in patients with recurrent glioblastoma. Sci. Transl. Med. *9*, eaaa0984.
6. Haas, A.R., Tanyi, J.L., O'Hara, M.H., Gladney, W.L., Lacey, S.F., Torigian, D.A., Soulen, M.C., Tian, L., McGarvey, M., Nelson, A.M., et al. (2019). Phase I Study of Lentiviral-Transduced Chimeric Antigen Receptor-Modified T Cells Recognizing Mesothelin in Advanced Solid Cancers. Mol. Ther. *27*, 1919–1929.
7. Annunziata, C.M., Ghobadi, A., Pennella, E.J., Vanas, J., Powell, C., Pavelova, M., Wagner, C., Kuo, M., Dansky Ullmann, C., Hassan, R., and Thaker, P.H. (2020). Feasibility and preliminary safety and efficacy of first-in-human intraperitoneal delivery of MCY-M11, anti-human-mesothelin CAR mRNA transfected into peripheral blood mononuclear cells, for ovarian cancer and malignant peritoneal mesothelioma. J. Clin. Oncol. *38*, 3014.
8. Richman, S.A., Nunez-Cruz, S., Moghimi, B., Li, L.Z., Gershenson, Z.T., Mourelatos, Z., Barrett, D.M., Grupp, S.A., and Milone, M.C. (2018). High-Affinity GD2-Specific CAR T Cells Induce Fatal Encephalitis in a Preclinical Neuroblastoma Model. Cancer Immunol. Res. *6*, 36–46.
9. Morgan, R.A., Yang, J.C., Kitano, M., Dudley, M.E., Laurencot, C.M., and Rosenberg, S.A. (2010). Case report of a serious adverse event following the administration of T cells transduced with a chimeric antigen receptor recognizing ERBB2. Mol. Ther. *18*, 843–851.
10. Bertolotti, A., Zhang, Y., Hendershot, L.M., Harding, H.P., and Ron, D. (2000). Dynamic interaction of BiP and ER stress transducers in the unfolded-protein response. Nat. Cell Biol. *2*, 326–332.
11. Lee, A.S. (2001). The glucose-regulated proteins: stress induction and clinical applications. Trends Biochem. Sci. *26*, 504–510.
12. Tsai, Y.L., Zhang, Y., Tseng, C.C., Stanciauskas, R., Pinaud, F., and Lee, A.S. (2015). Characterization and mechanism of stress-induced translocation of 78-kilodalton glucose-regulated protein (GRP78) to the cell surface. J. Biol. Chem. *290*, 8049–8064.
13. Misra, U.K., Gonzalez-Gronow, M., Gawdi, G., and Pizzo, S.V. (2005). The role of MTJ-1 in cell surface translocation of GRP78, a receptor for alpha 2-macroglobulin-dependent signaling. J. Immunol. *174*, 2092–2097.
14. Araujo, N., Hebbar, N., and Rangnekar, V.M. (2018). GRP78 Is a Targetable Receptor on Cancer and Stromal Cells. EBioMedicine *33*, 2–3.
15. Tsai, Y.L., Ha, D.P., Zhao, H., Carlos, A.J., Wei, S., Pun, T.K., Wu, K., Zandi, E., Kelly, K., and Lee, A.S. (2018). Endoplasmic reticulum stress activates SRC, relocating chaperones to the cell surface where

GRP78/CD109 blocks TGF-β signaling. Proc. Natl. Acad. Sci. USA *115*, E4245–E4254.

16. Limso, C., Ngo, J.M., Nguyen, P., Leal, S., Husain, A., Sahoo, D., Ghosh, P., and Bhandari, D. (2020). The Gα-interacting vesicle-associated protein interacts with and promotes cell surface localization of GRP78 during endoplasmic reticulum stress. FEBS Lett. *594*, 1088–1100.
17. Hebbar, N., Epperly, R., Vaidya, A., Thanekar, U., Moore, S.E., Umeda, M., Ma, J., Patil, S.L., Langfitt, D., Huang, S., et al. (2022). CAR T cells redirected to cell surface GRP78 display robust anti-acute myeloid leukemia activity and do not target hematopoietic progenitor cells. Nat. Commun. *13*, 587.
18. Farshbaf, M., Khosroushahi, A.Y., Mojarad-Jabali, S., Zarebkohan, A., Valizadeh, H., and Walker, P.R. (2020). Cell surface GRP78: An emerging imaging marker and therapeutic target for cancer. J. Contr. Release *328*, 932–941.
19. McLeod, C., Gout, A.M., Zhou, X., Thrasher, A., Rahbarinia, D., Brady, S.W., Macias, M., Birch, K., Finkelstein, D., Sunny, J., et al. (2021). St. Jude Cloud: A Pediatric Cancer Genomic Data-Sharing Ecosystem. Cancer Discov. *11*, 1082–1099.
20. Prinzing, B., Zebley, C.C., Petersen, C.T., Fan, Y., Anido, A.A., Yi, Z., Nguyen, P., Houke, H., Bell, M., Haydar, D., et al. (2021). Deleting DNMT3A in CAR T cells prevents exhaustion and enhances antitumor activity. Sci. Transl. Med. *13*, eabh0272.
21. Carnevale, J., Shifrut, E., Kale, N., Nyberg, W.A., Blaeschke, F., Chen, Y.Y., Li, Z., Bapat, S.P., Diolaiti, M.E., O'Leary, P., et al. (2022). RASA2 ablation in T cells boosts antigen sensitivity and long-term function. Nature *609*, 174–182.
22. Rossi, A., Pakhomova, O.N., Mollica, P.A., Casciola, M., Mangalanathan, U., Pakhomov, A.G., and Muratori, C. (2019). Nanosecond Pulsed Electric Fields Induce Endoplasmic Reticulum Stress Accompanied by Immunogenic Cell Death in Murine Models of Lymphoma and Colorectal Cancer. Cancers *11*, 2034.
23. Weber, E.W., Parker, K.R., Sotillo, E., Lynn, R.C., Anbunathan, H., Lattin, J., Good, Z., Belk, J.A., Daniel, B., Klysz, D., et al. (2021). Transient rest restores functionality in exhausted CAR-T cells through epigenetic remodeling. Science *372*, eaba1786.
24. Wang, S., Wei, W., Yuan, Y., Sun, B., Yang, D., Liu, N., and Zhao, X. (2023). Chimeric antigen receptor T cells targeting cell surface GRP78 efficiently kill glioblastoma and cancer stem cells. J. Transl. Med. *21*, 493.
25. Lieberman, N.A.P., DeGolier, K., Kovar, H.M., Davis, A., Hoglund, V., Stevens, J., Winter, C., Deutsch, G., Furlan, S.N., Vitanza, N.A., et al. (2019). Characterization of the immune microenvironment of diffuse intrinsic pontine glioma: implications for development of immunotherapy. Neuro Oncol. *21*, 83–94.
26. Jiang, Z., Zhang, G., Huang, L., Yuan, Y., Wu, C., and Li, Y. (2020). Transmissible Endoplasmic Reticulum Stress: A Novel Perspective on Tumor Immunity. Front. Cell Dev. Biol. *8*, 846.
27. Wei, C., Yang, X., Liu, N., Geng, J., Tai, Y., Sun, Z., Mei, G., Zhou, P., Peng, Y., Wang, C., et al. (2019). Tumor Microenvironment Regulation by the Endoplasmic Reticulum Stress Transmission Mediator Golgi Protein 73 in Mice. Hepatology *70*, 851–870.
28. Mahadevan, N.R., Rodvold, J., Sepulveda, H., Rossi, S., Drew, A.F., and Zanetti, M. (2011). Transmission of endoplasmic reticulum stress and pro-inflammation from tumor cells to myeloid cells. Proc. Natl. Acad. Sci. USA *108*, 6561–6566.
29. Cui, X., Zhang, Y., Lu, Y., and Xiang, M. (2022). ROS and Endoplasmic Reticulum Stress in Pulmonary Disease. Front. Pharmacol. *13*, 879204.
30. Malhotra, D., Shin, J., Solnica-Krezel, L., and Raz, E. (2018). Spatiotemporal regulation of concurrent developmental processes by generic signaling downstream of chemokine receptors. Elife *7*, e33574.
31. Rodvold, J.J., Chiu, K.T., Hiramatsu, N., Nussbacher, J.K., Galimberti, V., Mahadevan, N.R., Willert, K., Lin, J.H., and Zanetti, M. (2017). Intercellular transmission of the unfolded protein response promotes survival and drug resistance in cancer cells. Sci. Signal. *10*, eaah7177.
32. Choi, B.D., Yu, X., Castano, A.P., Bouffard, A.A., Schmidts, A., Larson, R.C., Bailey, S.R., Boroughs, A.C., Frigault, M.J., Leick, M.B., et al. (2019). CAR-T cells secreting BiTEs circumvent antigen escape without detectable toxicity. Nat. Biotechnol. *37*, 1049–1058.
33. Ma, Q., He, X., Zhang, B., Guo, F., Ou, X., Yang, Q., Shu, P., Chen, Y., Li, K., Gao, G., et al. (2022). A PD-L1-targeting chimeric switch receptor enhances efficacy of CAR-T cell for pleural and peritoneal metastasis. Signal Transduct. Targeted Ther. *7*, 380.
34. Lafleur, E.A., Koshkina, N.V., Stewart, J., Jia, S.F., Worth, L.L., Duan, X., and Kleinerman, E.S. (2004). Increased Fas expression reduces the metastatic potential of human osteosarcoma cells. Clin. Cancer Res. *10*, 8114–8119.
35. Furth, N., Algranati, D., Dassa, B., Beresh, O., Fedyuk, V., Morris, N., Kasper, L.H., Jones, D., Monje, M., Baker, S.J., and Shema, E. (2022). H3-K27M-mutant nucleosomes interact with MLL1 to shape the glioma epigenetic landscape. Cell Rep. *39*, 110836.
36. Milde, T., Lodrini, M., Savelyeva, L., Korshunov, A., Kool, M., Brueckner, L.M., Antunes, A.S.L.M., Oehme, I., Pekrun, A., Pfister, S.M., et al. (2012). HD-MB03 is a novel Group 3 medulloblastoma model demonstrating sensitivity to histone deacetylase inhibitor treatment. J. Neuro Oncol. *110*, 335–348.
37. Yu, L., Baxter, P.A., Voicu, H., Gurusiddappa, S., Zhao, Y., Adesina, A., Man, T.K., Shu, Q., Zhang, Y.J., Zhao, X.M., et al. (2010). A clinically relevant orthotopic xenograft model of ependymoma that maintains the genomic signature of the primary tumor and preserves cancer stem cells in vivo. Neuro Oncol. *12*, 580–594.
38. Milde, T., Kleber, S., Korshunov, A., Witt, H., Hielscher, T., Koch, P., Kopp, H.G., Jugold, M., Deubzer, H.E., Oehme, I., et al. (2011). A novel human high-risk ependymoma stem cell model reveals the differentiation-inducing potential of the histone deacetylase inhibitor Vorinostat. Acta Neuropathol. *122*, 637–650.
39. Schindelin, J., Arganda-Carreras, I., Frise, E., Kaynig, V., Longair, M., Pietzsch, T., and Cardona, A. (2012). Fiji: an open-source platform for biological-image analysis. Nature Methods *9*, 676–682.
40. Bonifant, C.L., Szoor, A., Torres, D., Joseph, N., Velasquez, M.P., Iwahori, K., Gaikwad, A., Nguyen, P., Arber, C., Song, X.T., et al. (2016). CD123-Engager T Cells as a Novel Immunotherapeutic for Acute Myeloid Leukemia. Mol. Ther. *24*, 1615–1626.
41. S., A. (2010). FastQC: A Quality Control Tool for High Throughput Sequence Data. Available online at: http://www.bioinformatics.babraham.ac.uk/projects/fastqc.
42. F, K. (2021). Trimgalore. Available at: https://github.com/FelixKrueger/TrimGalore.
43. Bray, N.L., Pimentel, H., Melsted, P., and Pachter, L. (2016). Near-optimal probabilistic RNA-seq quantification. Nat. Biotechnol. *34*, 525–527.
44. Team, R. (2020). RStudio (Integrated Development for R.RStudio, PBC). http://www.rstudio.com/.
45. Soneson, C., Love, M.I., and Robinson, M.D. (2015). Differential analyses for RNA-seq: transcript-level estimates improve gene-level inferences. F1000Res. *4*, 1521.
46. Kim, Y., Lillo, A.M., Steiniger, S.C.J., Liu, Y., Ballatore, C., Anichini, A., Mortarini, R., Kaufmann, G.F., Zhou, B., Felding-Habermann, B., and Janda, K.D. (2006). Targeting heat shock proteins on cancer cells: selection, characterization, and cell-penetrating properties of a peptidic GRP78 ligand. Biochemistry *45*, 9434–9444.
47. Mata, M., Gerken, C., Nguyen, P., Krenciute, G., Spencer, D.M., and Gottschalk, S. (2017). Inducible Activation of MyD88 and CD40 in CAR T Cells Results in Controllable and Potent Antitumor Activity in Preclinical Solid Tumor Models. Cancer Discov. *7*, 1306–1319.

48. Schindelin, J., Arganda-Carreras, I., Frise, E., Kaynig, V., Longair, M., Pietzsch, T., Preibisch, S., Rueden, C., Saalfeld, S., Schmid, B., et al. (2012). Fiji: an open-source platform for biological-image analysis. Nat. Methods *9*, 676–682.

49. Thiam, H.R., Vargas, P., Carpi, N., Crespo, C.L., Raab, M., Terriac, E., King, M.C., Jacobelli, J., Alberts, A.S., Stradal, T., et al. (2016). Perinuclear Arp2/3-driven actin polymerization enables nuclear deformation to facilitate cell migration through complex environments. Nat. Commun. *7*, 10997.

50. Ershov, D., Minh-Son, P., Joanna, W.P., Stéphane, U.R., Laure, L.B., Charles-Orszag, A., James, R.W.C., Romain, F.L., Nathan, H.R., and Daria, B. (2021). Bringing TrackMate into the era of machine-learning and deep-learning. Preprint at bioRxiv. https://doi.org/10.1101/2021.09.03.458852.

STAR★METHODS

KEY RESOURCES TABLE

REAGENT or RESOURCE	SOURCE	IDENTIFIER
Antibodies		
CD3	Miltenyi Biotec	Cat#130-093-337
CD28	Miltenyi Biotec	Cat#130-093-386
CD19-APC	BD Biosciences	Cat#555415
CD8-PerCP	Biolegend	Cat#344708
CD45RA-APC	Biolegend	Cat#304112
CCR7-FITC	Biolegend	Cat#353216
CD4-PE/Cy7	Biolegend	Cat#344612
PD1-PE	Biolegend	Cat#329905
TIM3-PE/Cy7	Biolegend	Cat#345013
LAG3-FITC	Biolegend	Cat#369307
HSPA5	Atlas antibodies	Cat#HPA038845
Isotype	Agilent DAKO	Cat#X090302
Biological samples		
Human peripheral blood mononuclear cells (PBMCs)	Deidentified healthy donors	St. Jude
Chemicals, peptides, and recombinant proteins		
rhIL-7	Peprotech	Cat#200-7
rhIL-15	Peprotech	Cat#200-15
rhFGF-b	Peprotech	Cat#100-18B
rhEGF	Peprotech	Cat#AF-100-15
B27	Thermofisher	Cat#12587010
N2	Thermofisher	Cat#17502048
GeneJuice	Novagen	Cat#70967
Heparin	Stemcell technologies	Cat#7980
Lymphoprep	Abbott Laboratories	Cat#07811
Retronectin	Clontech	Cat#T100B
Cas9	MacroLab	N/A
P3 Primary cell buffer	Lonza	Cat#V4XP-3032
Dasatinib	LC Labs	Cat#D-3307
LIVE/DEAD Aqua	Fisher Scientific	Cat#L34957
Celltracker Red CMTPX	Invitrogen	Cat#C34552
CAL520a.m.	ATTbioquest	Cat#21130
Celltrace Violet	Thermofisher	Cat#C34557
Matrigel	Corning	Cat#356234
Biotin-Ahx-CTVALPGGYVRVC	Genscript	N/A
Critical commercial assays		
13-plex human cytokine quantification kit	Millipore Sigma	Cat#HCYTOMAG-60K
IFN-gamma ELISA	R&D system	Cat#SMIF00
CellTiter96 Aqueous One Solution Cell Proliferation Assay	Promega	Cat#G3580
MycoAlert Mycoplasma detection kit	Lonza	Cat#LT07-318
Rneasy Plus Mini Kit	Qiagen	Cat#74134
Tissue array	Biomax	Cat#FDA999w3 and FDA331

(*Continued on next page*)

Continued

REAGENT or RESOURCE	SOURCE	IDENTIFIER
Experimental models: Cell lines		
293T	ATCC	Cat#CRL-3216
U373	ATCC	Cat#HTB-17
U87	ATCC	Cat#HTB-14
DAOY	ATCC	Cat#HTB-186
A673	ATCC	Cat#CRL-1598
D425	Sigma-Aldrich	Cat#SCC290
D341	ATCC	Cat#HTB-187
D283	ATCC	Cat#HTB-185
MDA-MB-468	ATCC	Cat#HTB-132
LM7	Eugenie Kleinerman[34]	MD Anderson
DIPG7	Suzanne Baker[35]	St. Jude
DIPG37	Suzanne Baker[35]	St. Jude
DIPG007	Suzanne Baker[35]	St. Jude
HGG42	Suzanne Baker[35]	St. Jude
HDMBO3	Till Milde[36]	KiTZ Heidelberg
MB002	Martine F. Roussel	St. Jude
1425	Stephen Mack (originally published by Litian Yu[37])	Texas Children's Cancer center
CPITT	Stephen Mack (unpublished)	St. Jude
ST1	Stephen Mack (unpublished)	St. Jude
EPI	Stephen Mack (originally published by Till Milde[38])	St. Jude
ST2	Stephen Mack (unpublished)	St. Jude
L46SJ	Stephen Mack (unpublished)	St. Jude
BT12	Anang A. Shelat	St. Jude
Experimental models: Organisms/strains		
NOD.Cg-Prkdc^{scid}IL2Rg^{tm1wjl}/SzJlnv (NSG)	St. Jude	N/A
Oligonucleotides		
RASA2 gRNA: AGGATCGACTTGTGGAACAA	Julia Carnevale[21]	N/A
AAVS1 gRNA: GGGAACCCAGCGAGTGAAGA	Brooke Prinzing[20]	N/A
Recombinant DNA		
GRP78-CAR	Velasquez Lab[17]	St. Jude
Ctrl-CAR	Velasquez Lab[17]	St. Jude
Software and algorithms		
GraphPad Prism 9.0	GraphPad software	https://www.graphpad.com
FlowJo 10.0	FlowJo, LLC	https://www.flowjo.com/
Living Image Software	Perkin Elmer	https://www.perkinelmer.com/
FIJI (ImageJ)	Schindelin et al.[39]	https://imagej.net/software/fiji/
Trackmate	Ershov D[40]	N/A
FastQC	Babraham Bioinformatics[41]	http://www.bioinformatics.babraham.ac.uk/projects/fastqc
Trimgalore	Felix Krueger[42]	https://github.com/FelixKrueger/TrimGalore
Kallisto	Bray N[43]	N/A
Rstudio	R team[44]	http://www.rstudio.com/
Txi-import	Soneson C[45]	N/A
HALO	Indica Labs	https://indicalab.com/halo/

RESOURCE AVAILABILITY

Lead contact

Request for further information and reagents should be directed to and will be fulfilled by the lead contact, Giedre Krenciute (giedre.krenciute@stjude.org).

Materials availability

Plasmids and cell lines used in this study can be made available under an appropriate materials transfer agreement (MTA). No other unique reagents were generated.

Data and code availability

- Data generated in this study is available from the lead contact upon request
- This paper does not report original code.
- Any additional information required to reanalyze the data reported in this work paper is available from the lead contact upon request.

EXPERIMENTAL MODEL AND SUBJECT DETAILS

Cell lines

The following cell lines were purchased from American Type Culture Collection (ATCC, Manassas, VA): 293T (female fetus), U373 (adult male), U87(adult male), DAOY (pediatric male), A673 (adult female), D425 (pediatric female), D341 (pediatric male), D283 (pediatric male) and MDA-MB-468 (MDA-468) (pediatric female). LM7 (pediatric female), osteosarcoma cells were kindly provided by Dr. Eugenie Kleinerman (MD Anderson Cancer Center). DIPG and HGG cell lines (DIPG7 [pediatric female], DIPG37 [pediatric male], DIPG007 [pediatric male], and HGG42 [pediatric male]) were kindly provided by Dr. Suzanne Baker (St. Jude Children's Research Hospital). Medulloblastoma cell lines (HDMB03[36] [originally from Dr. Till Milde] [pediatric male]), MB002 [pediatric male]) were kindly provided by Dr. Martine F. Roussel (St. Jude Children's Research Hospital). Ependymoma cell lines (1425 [pediatric male], CPITT [pediatric male], ST1 [pediatric female], EPI [pediatric female], ST2 [pediatric female], and L46SJ [pediatric male]) were kindly provided by Dr. Stephen Mack (St. Jude Children's Research Hospital). ATRT cell line (BT12 [pediatric female]) was kindly provided by Dr. Anang A. Shelat (St. Jude Children's Research Hospital). All cell lines were authenticated using the ATCC's or Hartwell center (St. Jude Children's Research Hospital) human STR profiling cell authentication service and routinely checked for Mycoplasma by the MycoAlert Mycoplasma Detection Kit (Lonza, Cat: LT07-318).

Cell line cultures

U373, BT-12, A673 and MDA-468 cells were maintained in RPMI-1640 (ThermoFisher, Cat: 21870076). U87 and DAOY cell line was maintained in EMEM media (ATCC, Cat: 30–2003). LM7 and 293T were maintained in Dulbecco's Modified Eagle Medium (DMEM) (GE Life Sciences, Cat: SH30081.01). All culture media listed above were supplemented with 10% Fetal Bovine Serum (FBS) (GE Life Sciences, Cat: SH30071.03) and GlutaMAX (2 mmol/L) (Gibco, Cat: 35050061). DIPG and HGG cell lines were cultured in Tumor Stem Media as described in.[35] Medulloblastoma (MB) cell lines were cultured in different culture media depending on the cell line: For HDMB03, D425, MB002, the media used was Neurobasal media (Thermofisher, Cat: 21103049) supplemented with 2 mmol/L GlutaMAX, 1X B27 (Thermofisher, Cat: 12587010), 0.00004% Heparin (Stemcell technologies, Cat: 7980), 20 ng/mL EGF (Peprotech, Cat: AF-100-15), and 20 ng/mL FGF-b (Peprotech, Cat:AF-100-15). For D341, the media used was EMEM supplemented with 20% FBS and 2 mmol/L GlutaMAX. For D283, the media used was EMEM supplemented with 10% FBS and 0.5 mmol/L GlutaMAX. Ependymomas (EPN) cell lines were cultured in Neurobasal media supplemented with 1mM Sodium Pyruvate (Thermofisher, Cat: 11360070), 2 mmol/L GlutaMAX, 1X B27, 1X N2 (Thermofisher, Cat: 17502048), 10 ng/mL EGF, and 10 ng/mL FGF-b. All cell lines were grown in humidified incubators at 37°C and 5% CO_2. LM7 and U87 cells were modified to express GFP-firefly luciferase (GFP.ffluc), MDA-468 cells were modified to express RFP-firefly luciferase (RFP.ffluc) by retroviral transduction as described.[40] DIPG007 cells were modified to express YFP-firefly luciferase (YFP.ffluc) by lentiviral transduction.

Primary human T cell culture and activation

This study was conducted with approval from the St. Jude Children's Research Hospital Institutional Review Board (IRB). T-cells were acquired from peripheral blood mononuclear cells (PBMCs) obtained from healthy donor de-identified apheresis products through a deidentified product protocol (23–1294 and NR17-114) and used in accordance with the Helsinki Declaration.

Peripheral blood mononuclear cells (PBMCs) were isolated using Lymphoprep (Abbott Laboratories, Cat: 07811) gradient centrifugation method. On day 0, PBMCs were stimulated on non–tissue culture–treated 24-well plates (Corning, Cat: 3738), which were precoated with CD3 and CD28 antibodies (αCD3/αCD28; Miltenyi Biotec, Cat: 130-093-337 [CD3: OKT3] and 130-093-386 [CD28: 15E8]). rhIL-7 (10 ng/mL; PeproTech, Cat: 200-7) and rhIL-15 (5 ng/mL; PeproTech, Cat: 200-15) were added to cultures on day 1. T cells were maintained in RPMI-1640 supplemented with 10% FBS, GlutaMAX (2 mmol/L), and rhIL-7 (10 ng/mL), rhIL-15 (5 ng/mL) cytokines were added every 3–4 days.

Animals

All animal experiments followed protocols (#627–100520 and #623–100650) approved by the St. Jude Institutional Animal Care and Use Committee (IACUC). Mice were euthanized when they met physical euthanasia criteria (tumor size, significant weight loss, signs of distress), or when recommended by St. Jude veterinary staff. For *in vivo* experiments, NSG mice were treated with CAR T cells generated from one to two different healthy donors. All experiments were performed using 10–12 weeks old male NOD.Cg-Prkdc^{scid}IL2Rg^{tm1wjl}/SzJlnv (NSG) mice. Female mice were excluded from the study because they did not meet weight and age criteria required for survival surgeries established and approved by IACUC. Cages of mice were randomly assigned to treatment groups. The technicians injecting and imaging the mice were not blinded to the names of treatment groups, but they were unaware of their meaning or expected results. The bioluminescence-defined endpoint (total flux greater than 1x10^{10} photons/second) or tumor volume endpoint (3000-4000mm^3) were selected to maximize animal welfare as larger tumor burdens were associated with clinical signs of pain and distress.

Brain tumor model

U87.GFP.ffluc or DIPG007.YFP.ffluc cells were implanted intracranially into NSG mice. For intracranial implantation, mice were anesthetized and placed in a stereotactic rodent surgery platform. The scalp was cut using surgical scissors, and a cranial window was made in the skull, over the right cortical hemisphere, by using a dental drill. A sterile, cold Hamilton syringe containing 3X10^4 U87.GFP.ffluc cells suspended in 5uL Matrigel (Corning, Cat: 356234) was placed in the stereotactic apparatus. The needle of the syringe was brought into contact with the surface of the brain, slowly inserted 2.5mm into the cortex, raised 0.5mm, and then the cells were injected over 1 min. The syringe was left in place for 45 s to prevent backflow. Wound clips were used to close the surgical site. 2x10^6 or 5x10^6 GRP78-CAR T cells were injected 7 days later in the same location in 2 or 5uL of PBS, respectively. Tumor burden was assessed weekly using bioluminescent *in vivo* imaging system (PerkinElmer, IVIS) until the humane endpoint was reached, and mice were euthanized.

Osteosarcoma model

1x10e6 LM7.eGFP.ffLuc cells were injected intraperitoneally on day 0. 5x10^5 GRP78-CAR T cells were injected 7 days later in the same location. Tumor burden was assessed weekly using bioluminescent *in vivo* imaging system (IVIS) until the humane endpoint was reached, and mice were euthanized.

TNBC model

5x10^5 MDA-MB-468.RFP.ffluc cells, suspended in PBS/Matrigel (1:1), were injected into the mammary fat pad. On day 7, mice received a single iv dose of 3x10^6 CAR T cells by tail vein injection. Tumor growth was monitored by weekly IVIS imaging, until the humane endpoint was reached, and mice were euthanized.

Ewing sarcoma model

5x10^5 A673 cells, suspended in PBS: Matrigel (1:1), were injected sc. On day 7, mice received a single iv dose of 3x10^6 or 1x10^7 CAR T cells by tail vein injection. A673 tumor growth was monitored by caliper measurements twice weekly. Mice were euthanized at predefined endpoints or when they met euthanasia criteria in accordance with SJCRH's Animal Resource Center.

METHOD DETAILS

Constructs and sequences

Generation of GRP78-CAR viral vector has been previously described.[17] Briefly, we synthesized cDNAs (GeneArt, ThermoFisher Scientific) encoding the IgG heavy chain leader sequence and one copy of the GRP78-specific peptide CTVALPGGYVRVC)[46] These were subcloned into a pSFG retroviral vector that encoded a mutant IgG4 hinge, a CD28 transmembrane domain, a CD28.CD3zsignaling domain, a T2A ribosomal skip sequence and truncated CD19 (tCD19) to enable detection of transduced cells. The control CAR (Ctrl-CAR) was generated by deleting the CD28.CD3ζ signaling domain from the GRP78-CAR. The sequence of all cloned constructs was confirmed by sequencing performed by Hartwell Center DNA Sequencing Core at St. Jude Children's Research Hospital with Big Dye Terminator (v3.1) Chemistry on Applied Biosystems 3730XL DNA Analyzers (Thermo Fisher Scientific, Cat: 4337454).

Retrovirus production and transduction

The generation of the RD114-pseudotyped retroviral particles has been previously described.[40] Briefly, retroviral particles were generated by transient transfection of HEK293T cells which were seeded at 1–2 million cells per 10cm dish 2 days before transfection and cultured in DMEM with 10% FBS. Cells were transfected with the CAR retroviral plasmid, retroviral packaging plasmids Peq-Pam3-E and a plasmid encoding the RD114 envelope protein using the GeneJuice transfection reagent per manufacturer's protocol (Novagen, Cat: 70967). 48h viral supernatants were collected, spun down at 400g for 5 min and filtered using 0.45μm filter to remove the cell debris. Viral supernatants were then snap-frozen and stored at −80°C until further use.

For T cell transduction, 500ul of viral supernatants were spun down on RetroNectin (Clontech, Cat: T100B) coated 24-well non-tissue culture plate at 2000g for 90min. After the spin, viral supernatants were removed and activated T cells (day 2) were plated

at 2.5x10^5 cells/well in 2 mL of RPMI 1640 supplemented with 10% FBS, 1% GlutaMAX, 10 ng/mL IL-7, and 5 ng/mL IL-15 T cell media (T cell media). 48h later, CAR transduced T cells were transferred from the RetroNectin-coated plate to a tissue culture plate and expanded in T cell media. CAR expression was determined 4 to 5 days post-transduction.

CRISPR-Cas9 knock-out genetic editing

Activated T cells were electroporated with Streptococcus pyogenes Cas9-sgRNA RNP complexes targeting RASA2 or AAVS1 (Ctrl), and 24 h later cells were transduced on RetroNectin-coated plates. RNPs were precomplexed at an sgRNA:Cas9 ratio of 4.5:1, prepared by adding 3 μL of 60 μM sgRNA (Synthego) to 1 μL of 40 μM Cas9 (MacroLab, University of California, Berkeley) and frozen for later use. For gene KO, 1 × 10e6 T cells were resuspended in 17 μL of P3 Primary cell buffer (Lonza, Cat: V4XP-3032) and added to 3 μL of RNP. 20 mL of cells + RNP were nucleofected by using EH-115 program in the Lonza 4D-nucleofector (Lonza). One electroporation reaction was collected in one well of a 48-well tissue culture–treated plate containing RPMI 1640 supplemented with 20% FBS, GlutaMAX, IL-7 (10 ng/mL), and IL-15 (5 ng/mL) for 72 h. After recovery, the medium was switched to RPMI 1640 containing 10% FBS and GlutaMAX. The cells were then expanded for 10 to 12 days with IL-7 and IL-15 added every 2 to 3 days at the same concentrations indicated above. Dasatinib (30 nM) (LC Labs, Cat: D-3307) was added to the culture medium 3 days after transduction and replenished every 48–72 h. Dasatinib was removed prior to *in vitro* and *in vivo* functional studies.

Flow cytometry

All flow cytometry data were acquired with a BD FACSCanto II instrument and analyzed using FlowJo software (FlowJo, Ashland, OR). Samples were washed with and stained in DPBS (Lonza, Basel, Switzerland) with 1% FBS (GE Life Sciences, Cat: SH30071.03). For all samples, matched isotypes or known negative controls, e.g., non-transduced (NT) T cells, served as gating controls. Invitrogen LIVE/DEAD Fixable Aqua Dead Cell Stain kit (Fisher Scientific, Cat: L34957) was used as a viability dye. For GRP78 expression cells were stained with a GRP78-specific peptide with an N-terminal Biotin tag (Biotin-Ahx-CTVALPGGYVRVC) was custom synthesized by Genscript (Piscataway, NJ) and used at 3 mM working concentration in combination with Streptavidin PE at 1:100 dilution. Cells were washed twice and then resuspended for flow cytometry analysis. The GRP78-CAR and Ctrl-CAR were detected with CD19-APC (BD Biosciences, Cat: 555415). T cell phenotype was assessed with: CD8-PerCP (Biolegend, Cat: 344708), CD45RA-APC (Biolegend, Cat: 304112), CCR7-FITC (Biolegend, Cat: 353216), CD4-PE/Cy7 (Biolegend, Cat: 344612). T cell exhaustion/activation was measured with: PD-1-PE (Biolegend, Cat: 329905), TIM-3-PE/Cy7 (Biolegend, Cat: 345013), and LAG-3-FITC (Biolegend, Cat:369307). All staining was performed for 15 min at room temperature in the dark.

Immunohistochemistry

Commercially available tissue arrays (US Biomax, Cat: FDA999w3 and FDA331) were used to assess the HSPA5 (GRP78) expression in normal tissues. And De-identified 5 mm formalin-fixed paraffin-embedded (FFPE) sections of ZFTA fusion-positive ependymoma, pontine H3 K27M-mutant diffuse midline glioma, and group 3 medulloblastoma patient samples. All tissue samples were processed, sectioned at 4-μm onto mounted on positive charged glass slides (Thermofisher, Cat: 22-037-246), and stained with hematoxylin and eosin (HE).

Staining for HSPA5 (GRP78) was done using a polyclonal HSPA5 antibody (Atlas antibodies, Cat: HPA038845) according to the established staining protocol (Comparative Pathology Core, St. Jude). Routine hematoxylin and eosin-stained sections were used to verify the presence of tumors before subjecting the FFPE sections to immunohistochemistry. An isotype control (Agilent DAKO, Cat: X090302) was used to confirm the specificity of immunoreactivity. A board-certified pathologists (HTS, JC) blindly interpreted tissue histology and conducted visual assessments of immunohistochemical stains for tissue microarrays.

After visual review histology slides were scanned to a 20x scalable whole slide image using a PANNORAMIC 250 Flash III slide scanner (3DHISTECH, Ltd.). The HALO image analysis program and the Multiplex IHC v2.3.4 algorithm (Indica Labs) was used to assess any differences in expression across normal human tissues, human gliomas, and human DIPG xenografts. HSPA5 expression was ubiquitous in all normal human tissues with variable staining patterns binned as blush/background (0+), weak (1+), moderate (2+), or strong/overstained (3+) in the algorithm based on visual assessments of staining intensity determined by the pathologists. Immunoreactivity was localized to the membrane and/or cytoplasm of all immune-positive cells in all sampled human adult and pediatric tissues.

Gene expression analysis

The gene expression data of Pediatric solid and brain tumors are from St. Jude cloud[19] and TARGET Childhood Cancer Program (Available at the Genomic Data Commons [https://portal.gdc.cancer.gov]). The gene expression data of adult tumors are from The Cancer Genome Atlas Program (TCGA) Research Network (https://www.cancer.gov/tcga). The gene expression data of normal tissue are from the Genome-Tissue Expression (GTEx) Portal (dbGaP accession number phs000424.v8.p2). The feature counts files from St. Jude cloud were used to generate the transcripts per million (TPM) value of gene expression through the tool cgp-convert-counts (https://github.com/cancerit/cgp-convert-counts) with default parameters. For the other cohorts, the TPM quantifications were obtained from the downloaded file available in the portal. Totally, 17,382 GTEx normal samples, 2,410 pediatric tumor samples (2,030 from St. Jude cloud and 380 from TARGET), and 9,094 adult tumor samples were used to quantify gene expression.

For gene expression analysis in cell lines, the RNA was extracted using the Rneasy Plus Mini Kit (Qiagen, Hilden, Germany). RNA samples were then sent for sequencing at the Hartwell Center (St. Jude). Sequencing quality was assessed by FastQC,[41] trimming by Trimgalore,[42] and mapping/quantification by Kallisto[43] using the Homo Sapiens Ensembl transcriptome v96. TPMs were obtained by loading the samples onto Rstudio,[44] by using txi-import package.[45]

Repeated stimulation assay

Ctrl and GRP78-CAR T cells were co-cultured with tumor cells at an effector to target ratio of 2:1. Three-Four days later, T cells were counted and replated with fresh tumor cells at the same 2:1 ratio. The T cells continued to be counted and stimulated with fresh tumor cells on a weekly basis until the T cells stopped killing tumor cells.

Cytokine production

At 24 h post first stimulation, culture supernatants were collected, and cytokine production was assessed by a 13-plex human cytokine quantification kit (Millipore Sigma, Cat: HCYTOMAG-60K). Analysis was performed using a Luminex FlexMap 3D instrument and software (Luminex Corporation). For IFN-γ, quantitative ELISA kits were used according to the manufacturer's protocol (R&D Systems, Cat: SMIF00).

Cytotoxicity assay

A CellTiter96 AQueous One Solution Cell Proliferation Assay (Promega, Cat: G3580) was utilized to assess CAR T cell cytotoxicity as previously described.[47] Briefly, tumor cells were incubated with varying amounts of CAR T cells to assess cytotoxicity at a range of E:T ratios. Twenty-four hours later, the media and T cells were removed, and the remaining tumor cells were quantified with the CellTiter96 AQueous One Solution Reagent containing a tetrazolium compound [3-(4,5-dimethylthiazol-2-yl)-5-(3-carboxymethoxyphenyl)-2-(4-sulfophenyl)-2H-tetrazolium, inner salt; MTS] and an electron coupling reagent (phenazine ethosulfate; PES). Media only and tumor only served as controls to assess percent cytotoxicity. Absorbance was measured at 492nm by using an Infinite200 Pro MPlex plate reader (Tecan, Männedorf, Switzerland). The percentage of live tumor cells was calculated suing the following formula: [(Absorbance of sample- Absorbance of media only)/(Absorbance of tumor only-Absorbance of media only)]x100.

Live cell imaging

$1.5x10^5$ tumor cells were seeded onto μ-slide 8 well chambers (Ibidi, Cat: 80807) and incubated overnight at 37°C and 5% CO2. Tumor cells were labeled with CellTracker Red CMTPX (1:1000) (Invitrogen, Cat: C34552) for 30 min and then washed and maintained in culture media until image acquisition. $2x10^6$ CAR T cells were resuspended in 1mL of PBS and labeled with CAL520 (1:500) (ATTbioquest, Cat: 21130) and CellTrace Violet (1:1000) (Thermofisher, Cat: C34557) for 1 h and then washed and maintained in T cell media until image acquisition. At a time of image acquisition, $3x10^5$ CAR T cells were added to each well preloaded with tumor cells, and the image acquisition was initiated once T cells were detected in the visual field. Images were acquired in a spinning disc confocal microscope (Zeiss Axio Observer with CSU-X spinning disc), using a 63× objective. The acquisition parameters were a 4D image (60 min of acquisition with 1 min of frame, and 20μm of height with a Z-step of 1μm).

The processing and analysis were performed with FIJI (ImageJ) software.[48] Cell tracking[49] and Ca^{2+} influx were performed using Trackmate plugin as described in.[50] All tumor and CAR T cell interactions were recorded over time, and Ca^{2+} influx was measured as the maximum fluorescence emitted by CAL520 signal which was normalized by its value before the first peak of calcium influx upon tumor interaction. Total Ca^{2+} influx was quantified as the area under curve. (AUC) of Ca^{2+} influx registry until 30 min of interaction.

Bioluminescence imaging

Mice were imaged by the St. Jude Center for *In Vivo* Imaging and Therapeutics (CIVIT). Mice were injected i.p. with 150 ng/kg of D-luciferin 5-10 min before imaging, anesthetized with isofluorane (1.5–2% delivered in 100% O2 at 1L/min), and imaged with Xenogen IVIS-200 imaging system (Xenogen, Alameda, CA). Quantification of tumor burden was performed using Living Image software (PerkinElmer). A region of interest (head for U87 and DIPG007, total body for A673, MDA-468 and LM7) was drawn around each mouse, and total flux was recorded in units of photons/second.

QUANTIFICATION AND STATISTICAL ANALYSIS

Statistical analysis

Statistical analyses were performed using GraphPad Prism 9.0 (Graphpad Software Inc, La Jolla, CA). Statistical analyses were only performed when the number of replicates was at least three. For comparisons of two groups, a paired or unpaired t-test was used. Two-tailed t-tests were performed in all instances unless otherwise specified in the figure legend. For comparisons of three or more groups, a one- or two-way analysis of variance (ANOVA) was used followed by either Dunnett's, Sidak's or Tukey's multiple comparisons test. Survival data were analyzed using a log rank (Mantel-Cox) test. For all experiments, p values less than 0.05 were considered significant.